Prescribed Fire Simulation with Dynamic Ignitions using Data from UAS-based Sensing

Xiaolin Hu[A,D], Mu Ge[A], Saket Gowravaram[B], Haiyang Chao[B], Ming Xin[C]
[A]Department of Computer Science, Georgia State University, Atlanta, GA 30303, USA
[B]Department of Aerospace Engineering, University of Kansas, Lawrence, KS 66045, USA
[C]Department of Mechanical and Aerospace Engineering, University of Missouri, Columbia, MO 65211, USA
[D]Corresponding author. Email: xhu@gsu.edu

ABSTRACT
Prescribed fire is an important tool for wildfire management and land management. Simulation of prescribed fires holds great potential in supporting planning of prescribed burn events. This paper presents a simulation-based study of a prescribed fire using data from Unmanned Aircraft System (UAS)-based sensing. A systematic approach for modeling and simulating prescribed fires with dynamic ignitions is developed. The developed approach is applied to a real prescribed fire where a UAS was used to monitor and collect data about the fire. The dynamic ignition process from multiple fire setting teams is specified, and simulation results are compared to real measurement data from UAS-based sensing. The results demonstrate the effectiveness of the developed modeling approach as well as the utility of using UAS-based fire measurements for prescribed fire simulations.

Keywords:
Prescribed fire, Wildfire, Dynamic ignition, Prescribed fire simulation, Fire spread simulation, Unmanned aircraft system, Sensing

1. Introduction

Prescribed fires, also known as prescribed burns or controlled burns, refer to the controlled application of fire by a team of fire experts under specified conditions to meet certain management objectives (USDA, n.d.). Prescribed fires can serve multiple purposes in wildland management, including protecting prairies from invasive overgrowth and removing hazardous fuels to reduce wildfire risk (Matthias et al. 2009, Fernandes & Botelho 2003). Prescribed burning is a complex activity that often involves multiple crews and equipment igniting fires at pre-determined locations of the fire area. The multiple ignitions, together with the spreading fire front, add complexity to the fire growth behavior. To carry out prescribed burning in a safe and controllable manner, effective planning of prescribed fires is essential (Waldrop and Goodrick 2012). Simulation of prescribed fires holds great potential in supporting learning and planning of prescribed fires. A comprehensive review of the various fire spread simulation models can be found in Sullivan (2009a, 2009b). Hiers et al. (2020) argued that existing simulation models in wildfire spread rely on assumptions that are not necessarily true for prescribed fires, mainly due to the smaller scale and the multiple ignition lines of prescribed fires. Linn et al. (2020) developed a coupled fire-atmospheric modeling tool for prescribed fire planning and showed simulation results.

A unique characteristic of prescribed fires is that they are ignited dynamically by fire setting teams. This compares to wildfires whose fire growth is mainly driven by the spread of fire fronts. Prescribed fire ignition plays a crucial role in the safety and effectiveness of prescribed burning. Martin and Dell (1978) summarized six firing techniques that are used in prescribed burning, including backfire, head fire, strip head fire, spot head fire, flank fire, and center or ring fire. These firing techniques serve as a basis to guide prescribed fire ignitions under various conditions (see, e.g., Bugwood Center, 1989). Besides ground ignition, prescribed fires may also be ignited through aerial ignition. In particular, in recent years Unmanned Aircraft System (UAS) has been used to assist prescribed fire ignition (Twidwell et al. 2016; Beachly 2017). The various ignition techniques for prescribed fires can significantly impact fire behavior and burn results. Finney and McAllister (2011) discussed how the different firing techniques may restrict or enhance

fire front interactions to result in different fire behavior. Johansen (1987) evaluated the differences that could occur in prescribed burning depending on whether lines of fire were used or a spot-fire technique is used. Besides ignition techniques, the complexity of prescribed fire ignition is also related to the configuration of multiple fire setting teams. Each team may have its own route, schedule, and ignition speed, all of which influence how a prescribed fire spreads. A systematic way of modeling the dynamic ignition of prescribed fires is needed for supporting prescribed fire simulation.

Aligning fire spread simulation with real data is of interest to many researchers (Kim et al. 2012, Sargent 2013). Kelso et al. (2015) presented a methodology for validating fire spread simulation systems using historical fire data, and demonstrated the methodology in a case study of simulating a large wildfire in Western Australia. Dahl et al. (2015) presented a coupled fire-atmosphere model for wildfire spread and applied it to simulation of a historical fire that burned 16,000 acres. Toivanen et al. (2019) compared results of a coupled atmosphere-fire simulation model with observed fire boundaries of the Black Saturday Kilmore East Wildfires. These works used data from large historical wildfires. The FireFlux experiments (Clements et al., 2007, 2019) collected field data for controlled grass fires, which have been simulated by several simulation studies (e.g., Kochanski et al. 2013; Filippi et al. 2013). A set of field measurements for a Mediterranean shrub fire were collected to characterize the fire behavior and evaluate physics based models of fire spread (Santoni et al. 2006, Morandini et al. 2006). More recently, Fayad et al. (2023) reported data for two experimental fires on a mountain shrubland and applied numerical simulations to study the rate of spread and fireline intensity of the fires. None of these works focused on the dynamic ignition of prescribed fires or studied the impact of different ignition techniques.

Collecting real time data of prescribed fires has been a challenging task. Traditional wildfire data collection methods such as satellites, manned aircraft, and ground fire sensors (e.g., ground towers) all have limitations for prescribed fire sensing. For example, satellite data typically have coarse spatial and temporal resolutions and are not suitable for small-scale prescribed fires; manned aircraft have limitations in terms of mission duration, mission safety, and cost; and ground fire sensors are difficult to deploy and can be damaged by fires. On the other hand, UAS technologies have advanced rapidly in recent years and become a viable option for prescribed fire data collection. UAS has the ability to fly on demand, operate in situations that are dangerous or too costly for manned aircraft, and continuously monitor an area to collect high resolution data. These features make UAS a desirable technology to collect real-time data for prescribed fires.

This paper presents a case study of prescribed fire simulation with dynamic ignitions using remote sensing data collected by UAS. A systematic approach for modeling and simulating prescribed fires with dynamic ignitions is developed to work with a underlying discrete event fire spread simulation model. The developed approach is applied to simulating an actual prescribed fire. We describe the UAS-based sensing for the prescribed fire, and characterize the prescribed fire growth behavior and dynamic ignition procedure based on the UAS data. Simulations are set up to simulate the prescribed fire, and simulation results are compared to real fire measurements from UAS. This paper makes contributions by focusing on the dynamic ignition in prescribed fire simulation and aligning the simulation study with real measurement data from UAS-based sensing. The developed modeling approach provides a systematic way to model and simulate prescribed fires that are dynamically ignited by multiple fire setting teams. The case study also shows how UAS can be used to collect data to support prescribed fire simulations. As there are growing interests in applying UAS to wildland fire management, this work demonstrates the utility of using UAS-based sensing to support wildland fire simulations.

2. Materials and Methods

2.1 The Prescribed Fire Simulation Model

The prescribed fire simulation is based on a discrete event simulation model that includes two components: a fire spread simulation model and a prescribed fire ignition model. The former models the fire spread behavior and the latter defines the dynamic ignitions of a prescribed fire.

The fire spread simulation model is based on DEVS-FIRE (Ntaimo et al. 2008; Hu et al. 2012). DEVS-FIRE is a discrete event simulation model for surface wildfire spread simulation and fire suppression simulation, built on the Discrete Event System Specification (DEVS) (Zeigler et al. 2000). In DEVS-FIRE the fire area is modeled as a two-dimensional cell space of individual cells with the fuel, terrain, and weather conditions assumed to be uniform within a cell. Each cell performs its local computation of the rate of spread and direction based on its fuel, terrain, and prevailing weather conditions. Except for the boundary cells, each cell is coupled with its eight surrounding neighbors. All cells are coupled to a weather model to receive weather data (wind speed and wind direction) that may change over time. Fire spread is modeled as a propagation process as burning cells ignite their unburned neighbor cells. When a cell is ignited, the fire spread speed of a cell is calculated using Rothermel's model (Rothermel 1972), which is a semi-empirical mathematical model that describes the fire behavior through equations derived from thermodynamic principles. The rate of spread is then decomposed into eight directions corresponding to its eight neighbors based on an elliptical shape that is computed based on the mid flame wind speed and the fire spread rate. Another example of using the cellular automata-based approach for modeling and simulating wildfire spread can be found in Trunfio et al. (2011).

The prescribed fire ignition model includes an ignition plan specification and a set of agent models that carry out the ignition plan. The ignition plan specification specifies an ignition plan that takes into consideration the following factors in dynamic ignition: 1) ignition team setting that describes if there are multiple teams of crew members igniting different parts of a fire; 2) ignition routes that describe the specific routes for igniting a fire; 3) ignition speeds that describe the moving speeds of ignition teams; and 4) ignition schedule that describe the timing of ignition activities, e.g., starting time of a specific segment, break time, etc. The ignition plan specification captures all these factors in a formal way. Specifically, we view that an ignition plan is composed of multiple teams. Each team ignites one or more segments of the fire. A segment of ignition is a straight line connecting a start location and an end location in the fire area that needs to be ignited. After finishing a segment, a team may wait for a period of time before igniting a new segment. The ignition plan ends after all teams finish their ignition segments. Without loss of generality, we use the following specification to specify an ignition plan.

<Team> *team_id*
  <Wait> *wait_time*
   start_location; end_location; speed; mode (continuous || spot)
  …
   start_location; end_location; speed; mode (continuous || spot)
  <Wait> *wait_time*
   start_location; end_location; speed; mode (continuous || spot)
  …
   start_location; end_location; speed; mode (continuous || spot)
</Team>

In the specification, the <*Team*> tag indicates the start of an ignition team, and the <*/Team*> tag indicates the end of the team. Each team has a unique identifier, denoted as *team_id*, which is an integer number. A statement starting with the <*Wait*> tag specifies the wait time (in seconds) between two segments, i.e., the break time between the end of the previous segment and the start of the next segment. A segment is specified by a statement starting with the <*Segment*> tag. Each segment has a start location (denoted as *start_location*), an end location (denoted as *end_location*), an ignition speed (denoted as *speed*, in m/s), and an ignition mode that can be either *continuous* or *spot*. A *continuous* mode means the segment is continuously ignited when the ignition team moves through the segment. A *spot* mode means fires are ignited as a line of spots rather than a continuous line of fire. The spot mode has an extra parameter

spot_distance to specify the distance (in meters) between two consecutive spots. For simplicity, this parameter is not shown in the specification above.

Based on an ignition plan, each fire setting team is modeled as an ignition agent that is implemented as a DEVS atomic model. Since DEVS-FIRE uses a cell space to model a fire area, an ignition agent ignites cells as it moves through the cell space. Each ignition agent has its own ignition route, schedule, and moving speed, which are derived from the ignition plan specification. When an agent moves across the cell space, it is dynamically coupled to the cells on its route and sends ignition messages to the cells to ignite them. Multiple agents are created to model multiple ignition teams. Once a cell is ignited by an ignition agent, it becomes a burning cell and will ignite its neighbor cells as part of the fire spread process defined by the fire spread simulation model. In the meantime, the agent may move to another cell to continue the ignition. More details about the ignition plan specification and how the ignition agents are implemented can be found in Hu and Ge (2021).

An illustration of an ignition agent and its connection to the cell space of DEVS-FIRE (only one ignition agent is illustrated) is shown in Figure 1(a), and an illustration of a fire spread simulation using the DEVS-FIRE model is shown in Figure 1(b).

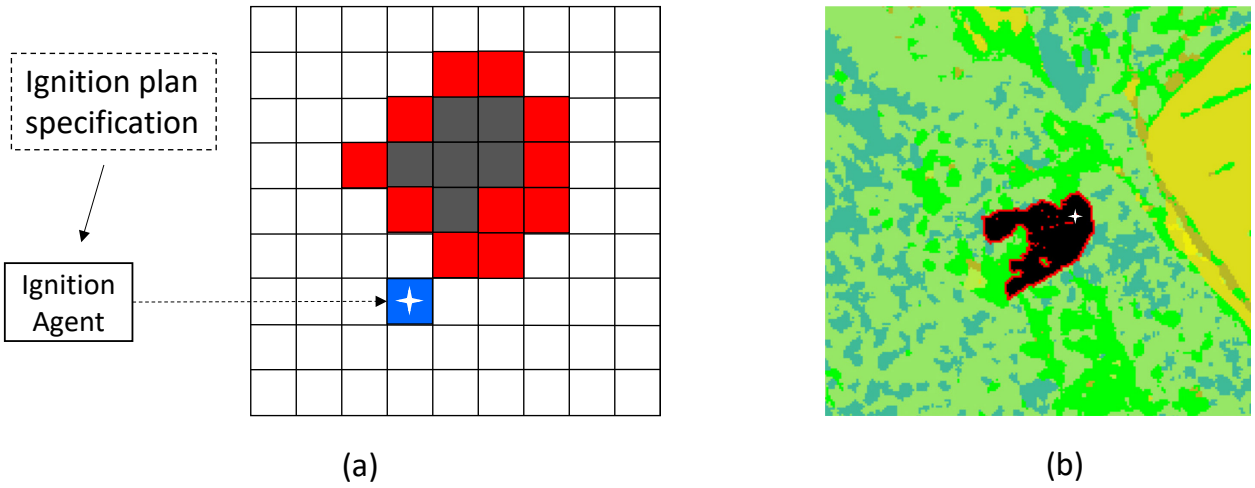

Figure 1. Ignition Agent and Fire Spread Simulation: (a) Illustration of ignition agent and its connection to the cell space model. White cells are unburned cells; red cells are burning cells; black cells are burned cells. The ignition agent is coupled to a blue cell with a white spark, indicating that the cell is ignited by the ignition agent. (b) Illustration of a fire spread simulation using the DEVS-FIRE model. The fire is ignited using a point ignition indicated by the while spark. Different colors (except for black and red) represent different fuel types. For better visual effect the grid lines of the cell space are not displayed.

2.2 Overview of the Prescribed Burn Event

The prescribed burn was conducted on October 8th, 2019 by the University of Kansas Field Station, with the purpose of promoting vegetative diversity and suppressing invasive species. The study area is a rectangular grassland field of about 530 meters long and 250 meters wide in the Anderson County Prairie Preserve in Kansas, as shown in Figure 2(a). Before the prescribed fire, the grass surrounding the study area was mowed and removed. This ensured the fire spread only inwards after ignition. The field is roughly flat. It rained several days before the fire burning. During the prescribed fire burning, the weather condition was sunny, with south wind at about 5-6 meters per second.

(a) (b)

Figure 2. Prescribed Fire Area and the KHawk UAS: (a) Prescribed fire area and fire setting routes (illustrated by the red lines in figure); (b) KHawk Zephyr 55 Thermal UAS.

The prescribed burn was carried out following a ring fire pattern along the field boundary. The fire setting crews started the fire on the north border at around 11:38 AM. They were divided into two teams to set the fire along the field boundary. The two teams met at the southern border at around 12:20 PM, and the prescribed fire ended at around 12:30 PM. During this period of time, each team set fires as they moved along the boundary of the study area (clockwise for the east team and counterclockwise for the west team). The fire setting routes of the two teams are illustrated in Figure 2(a). The fire setting followed the illustrated routes in a sequential order but with some variations. For example, the east team cut across the northeast corner while setting the fire there; this is marked by the dashed red line on the northeast corner of the field. The west team skipped some segments of the south side of the northwest corner. The two teams set fires at their own paces that varied over time, and both teams took short breaks during the fire setting process. Unfortunately, the detailed fire setting procedures were not documented; and no GPS receiver was used to track the locations of the fire setting teams. In this work, we characterize the ignition procedures of the two teams based on the fire front data sensed by the UAS (details provided later). Due to the strong wind that blew from south to north, the fire spread slowly when it was first ignited on the north side and then on the west and east sides. The most active part of the spreading happened when the fire setting teams arrived at the south side of the fire area.

2.3 UAS-Based Sensing

To monitor the prescribed fire, we used a fixed wing UAS named as the KHawk 55 Thermal UAS developed at the University of Kansas. Figure 2(b) shows the KHawk UAS. The KHawk UAS has two remote sensing payloads installed including a FLIR Vue Pro R thermal camera and a modified GoPro NDVI camera. The spectral band of the FLIR Vue Pro R camera is 7.5-13.5 μm and the sensor resolution is 640 by 512 pixels. During the prescribed fire, the KHawk UAS flew over the fire area at about 120 meters above the ground level to monitor the fire. Two flights were carried out with each flight lasting about 12-15 minutes. The first flight started about 6 minutes after the fire started and there was 15 minutes break time between the two flights. In the remainder of this paper, the two flights are referred to as *Flight1* and *Flight2*, respectively. In each flight, the UAS looped around the fire area to monitor the fire. The Flight1 had five loops and the Flight2 had four loops of flying.

The collected thermal images are used to extract fire front of the prescribed fire. The thermal camera was down-facing and took pictures at a 1 Hz frame rate. Due to the limited field of view and resolution of the thermal camera, each thermal image covered only a small portion of the prescribed fire area. To obtain a full image of the prescribed fire, the collected imagery data were orthorectified into aerial maps of the whole field using the Agisoft Photoscan Pro software. Because the UAS looped around the fire area to

monitor the fire, we grouped the thermal images according to the loops that the UAS flied. The images belonging to the same loop are stitched into a large orthorectified image to represent the full map of the prescribed fire at the time of the corresponding loop. Details about how the thermal images are processed and georeferenced can be found in Gowravarama et al. (2022). Note that a stitched thermal map is not a snapshot of the fire at a specific time because the images used to stitch the map were taken at different time instants while the fire was spreading. Nevertheless, because each loop spanned a relatively short period of time (about 2-4 minutes), we use the stitched thermal maps as the "ground truth" for the prescribed fire.

Not all loops produced enough thermal images to stitch a full map. Figure 3 shows the stitched maps from Flight1's Loop1, Loop 3, and Loop 4 (the top row) and Flight2's Loop2, Loop 3, and Loop 4 (the bottom row). Each loop has an ending time that is the elapse time from when the prescribed fire was first ignited. During Flight1, the fire was ignited only on the north boundary of the fire area. The fire line expanded to east and west due to ignitions from the fire setting teams. During Flight2, the maps show that by the end of Loop 2 the west fire setting team had ignited a portion of the south border and the east team was still on the east border; by the end of Loop 3 the east team had reached the south border; and by the end of Loop 4 the whole south border had been ignited. Note that the Loop 2 map has several regions (displayed in black) where information was missing due to lack of quality thermal images. The Loop 4 map marks the location where the two teams merged and ended their fire setting routes. We refer to this location as the *Merging Point* of the two fire setting routes. Because the UAS had only two flights for the prescribed fire, the Flight2's Loop 4 map data was the last data that is available from the UAS-based sensing.

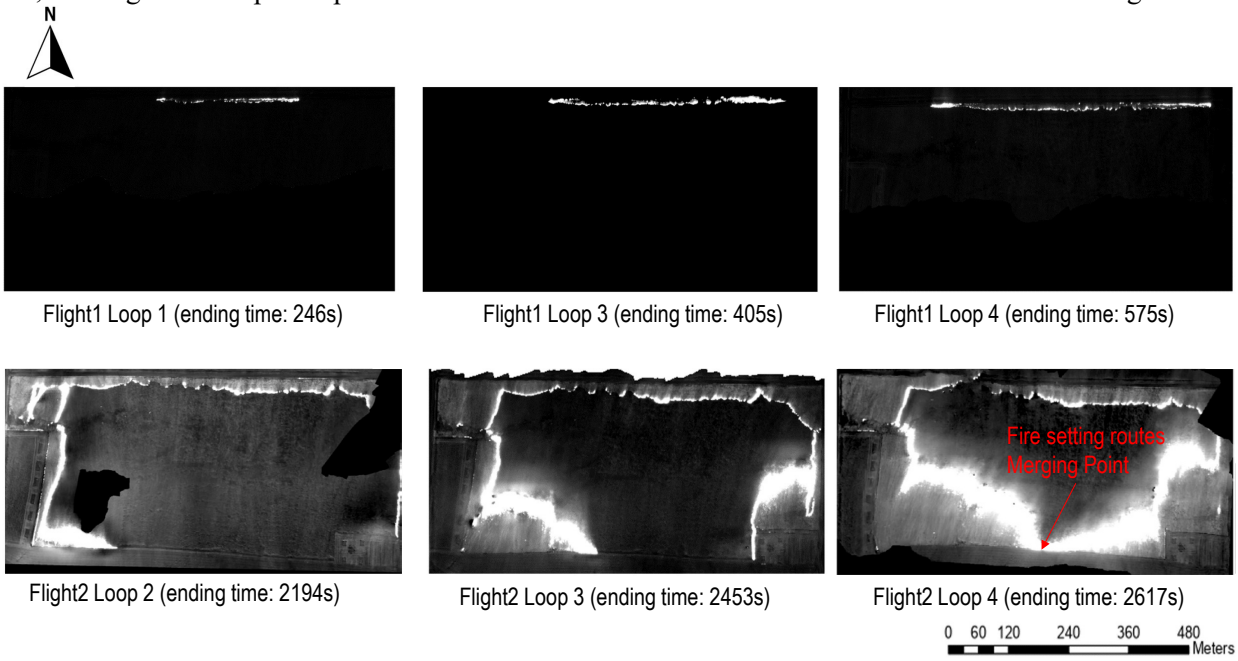

Figure 3: Thermal maps of the prescribed fire from Flight1 and Flight2 (white color represents the burning fire front of the prescribed fire)

The stitched thermal maps allow us to extract the fire fronts and display them on a 265 × 140 cell space (with cell size of 2 meters) used for the prescribed fire simulations. These fire fronts are considered as the real fire fronts in this paper. Figure 4 shows the extracted fire fronts In the figure, the red dashed lines on the south side indicate the routes of the two fire setting teams between the Loop2 ending time and Loop 4 ending time. During this time, the west fire setting team ignited fires from location A to location M; the east team ignited fires from location B to location C, and then to location D, and to location M. The location M is the merging point marked in Flight2's Loop 4 map in Figure 3. Each location is mapped to a specific cell on the cell space (the cell at the bottom left corner has coordinate of (0, 0)). The cell coordinates of

these locations are: A=(79, 14); B=(256, 30); C=(215, 30); D=(215, 14); M=(129, 14). We also marked several places (referred to as *Gap1*, *Gap2*, and *Gap3*) of the fire fronts that will be used in Section 3.1 to help determining the fire setting procedures.

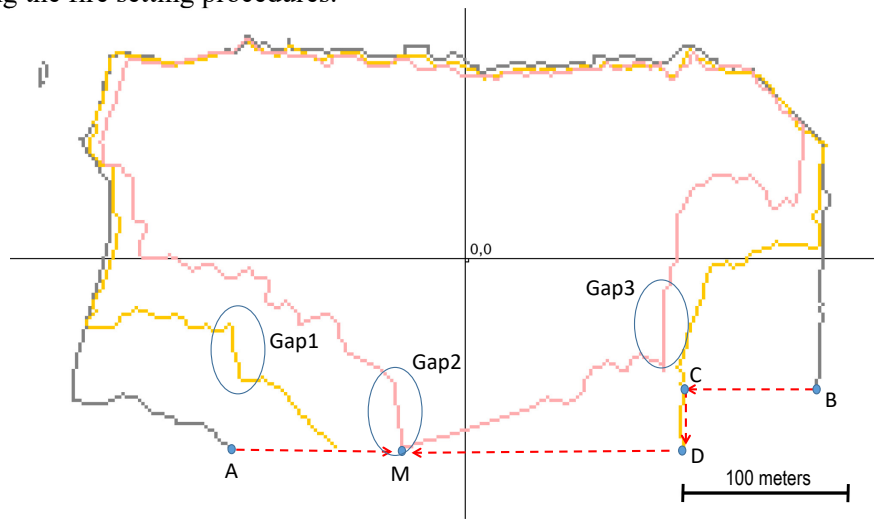

Figure 4: Extracted fire fronts from Flight2' Loop 2, Loop 3, and Loop 4 thermal maps, displayed in gray, orange, and pink, respectively. The red dashed lines on the south side indicate the routes of the two fire setting teams between the Loop2 ending time and Loop 4 ending time.

Based on the extracted fire front, we can estimate the *forward rate of spread* (FROS) of the fire, which is the rate of spread of the fire in the direction of the prevailing wind. For this fire event, the prevailing wind direction was from south to north. To compute the FROS, we use the Flight2's Loop 3 and Loop 4 fire front data to measure the north spreading distances of multiple locations and then divide them by the time of spreading. This resulted in an average FROS of 0.41 m/s, which is used as the representative FROS of the prescribed fire.

2.4 Simulation Setup

To simulate the prescribed fire, we set up a 265 × 140 cell space with cell size of 2 meters. The cell space is aligned with the geo-location of the fire area and covers the entire area. To run fire spread simulations using the DEVS-FIRE model, the following data are needed: 1) terrain data; 2) weather data; 3) fuel data, and 4) fire ignition procedure.

The terrain of the prescribed fire area is mostly flat. To obtain the specific terrain data (slope and aspect), we downloaded the LIDAR data corresponding to the fire area from the USGS Lidar Point Cloud (LPC) that is a part of the 3D Elevation Program (3DEP) (USGS, n.d.). The LIDAR data was published by USGS on July 28, 2016 at a native ground sampling distance (GSD) of 1.4 meter and 4 multiple discrete returns, which was then processed using ArcMap and presented at 2-meter resolution that matches the 2-meter cell size in the DEVS-FIRE model.

The weather data include wind speed and direction, both of which changed dynamically over time. During the prescribed fire, we set up a Campbell Scientific CSAT3B 3D sonic anemometer near the burning field. The anemometer measured real time 3D wind at 100Hz at ~1.9 meters above the ground. The wind speed measured at this height is consistent with the *midflame wind speed* used by Rothermel's model (Andrews 2012). The raw wind data was filtered by a 20-second moving average filter. The filtered data was further processed according to the 1-minute time interval by averaging the data points within each 1-minute interval and then used in the DEVS-FIRE model. During the prescribed fire the wind speed varied between 4 m/s and 8 m/s with an average of 6.03 m/s; the wind direction was centered around degree 0 (corresponding to the prevailing wind direction from south to north) with a variation up to ±20 degrees.

The overall effect of the wind was to drive the prescribed fire to spread the fastest to the north direction. In the simulations, we assume all cells share the same wind conditions (i.e., no spatial heterogeneity).

The fuel data describe the vegetation type and related fuel properties. The prescribed fire area was a grassland field covered by tall grass at the height of ~1.5 meters. Following the guidelines in Scott and Burgan (2005), we choose GR8 (representing high load, very coarse, humid climate grass) as the fuel model for the fire area and assume homogenous fuel conditions across the whole area. The GR8 fuel model is a dynamic fuel model, meaning that its herbaceous load shifts between live and dead depending on the specified live herbaceous moisture content. The fuel moisture content values (percentage) for both the dead and live fuels are important parameters of the fuel model. In this work, we tune the fuel moisture content values based on the observed FROS from the real fire. As the result of this tuning, the dead fuel moisture content values are set as 9% (1-hr), 11% (10-hr), 12% (100-hr) (corresponding to the Moderate moisture scenario for dead fuel as described in Scott and Burgan (2005)). The live fuel moisture content value is set as 75% for live herbaceous (corresponding to the one-half cured scenario for live fuel). With these fuel moisture content values, the fire behavior model produces a FROS that matches the representative 0.41 m/s FROS observed in the real field.

The fire ignition procedure is a key factor driving the fire growth and thus needs to be specified. As described before, the fire setting routes of both the east and west teams followed the fire area borders, started on the north side and ended on the south side. Unfortunately, the specific fire setting procedures of the two teams were not documented. In this work we characterize the ignition procedures of the two teams, including the specific ignition segments and speeds, waiting locations and time, based on the overall ignition routes and how the fire progressed. We then specify the major ignition activities using the developed ignition plan specification and run simulations. More details are provided below.

3. Simulation Results

3.1 Prescribed Fire Simulation for the Flight2 Time Period

Our first simulation considers the time period between Flight2's Loop 2 ending time and Loop 4 ending time. During this time period (423 seconds) the fire was ignited at the south border and spread fast toward north (see Figure 3). The simulation uses Flight2's Loop 2 map as the initial condition and runs for 423 seconds to end at the Loop 4 ending time.

During this time period, the west and east fire-setting teams ignited fires along their corresponding routes illustrated in Figure 4. The west team ignited the segment A-M; the east team ignited the segments B-C, C-D, and D-M in a sequential order. For the west team, the southwest part of the Loop 3 fire front shows a vertical cliff shape (marked as *Gap 1* in Figure 4) to the north of location A. This indicates a time gap between igniting the left and right segments of location A at the south border. Similarly, the Loop 4 fire front shows a vertical cliff shape (marked as *Gap 2*) to the west of location M (the merging point). This means the west team finished igniting the A-M segment earlier than when the east team finished igniting the D-M segment. Based on the above analysis, we estimate the major ignition activities of the west team as below: it started by waiting at location A for 120 seconds, and then ignited segment A-M with a speed of 0.45 m/s. The west team arrived at location M 76 seconds ahead of the Loop 4 ending time. For the east team, the southeast part of the Loop 4 fire front shows a vertical cliff shape (marked as *Gap 3*), indicating that the east team waited at location D for some time before continuing igniting the segment D-M. Based on this analysis, we estimate the major ignition activities of the east team as below: it started by igniting segments B-C and C-D at a speed of 1.3 m/s, and then took a 200-second break at location D before finishing igniting segment D-M at the speed of 1.3 m/s. The east team arrived at location M right at the Loop 4 ending time. We note that in reality the two fire setting teams ignited fires at their own paces that varied over time. Our goal here is to characterize their major ignition activities as opposed to reproducing every details of their ignition movements.

The left column of Table 1 shows the ignition plan specification for the estimated fire setting procedure described above. For comparison purpose, we also simulate a "non-stopping average speed" ignition scenario where both teams ignite fires at constant speeds and arrive at the merging point (Location M) at

the same Loop 4 ending time. The constant speeds are calculated as the average speeds by dividing their moving distances (the distance of segment A-M for the west team; the distance sum of segments B-C, C-D, and D-M for the east team) by the overall time duration (423 seconds). The ignition plan specification for this "non-stopping average speed" scenario is shown in the right column of Table 1.

Table 1: Ignition Plan Specification for the Flight2 Time Period

The estimated procedure	The "non-stopping average speed" procedure
<Team> *0 // west team* <Wait> *120* *A; M; 0.45; continuous* </Team> <Team> 1 // east team B*; C; 1.3; continuous* C*; D; 1.3; continuous* <Wait> *200* D*; M; 1.3; continuous* </Team>	<Team> *0 // west team* *A; M; 0.24; continuous* </Team> <Team> 1 // east team B*; C; 0.68; continuous* C*; D; 0.68; continuous* D*; M; 0.68; continuous* </Team>

We run simulations to simulate the prescribed fire using the two ignition plan specifications in Table 1. Figure 5(a) and 5(b) show the simulated fire fronts at the Loop 3 ending time and Loop 4 ending time, respectively. As can be seen, the simulated fire front using the estimated ignition procedure (blue) captures the main features of the real fire front well, except for the central west area where the simulated fire spreads faster than the real fire did. This difference is likely due to the fact that the actual fuel in that area differs from what was used in the simulation, which made the real fire in that area spread slower. Comparing the simulated fires using the two ignition procedures, we can see that the two procedures result in different fire shapes. The fire using the estimated ignition procedure matches the real fire front more accurately. For example, by the Loop3 ending time, the estimated ignition procedure makes the east team arrive at the south border but has not ignited any part of it yet (this is the same as being observed from the real fire); whereas the "non-stopping average speed" ignition procedure makes the east team ignite a portion of the south border already by that time.

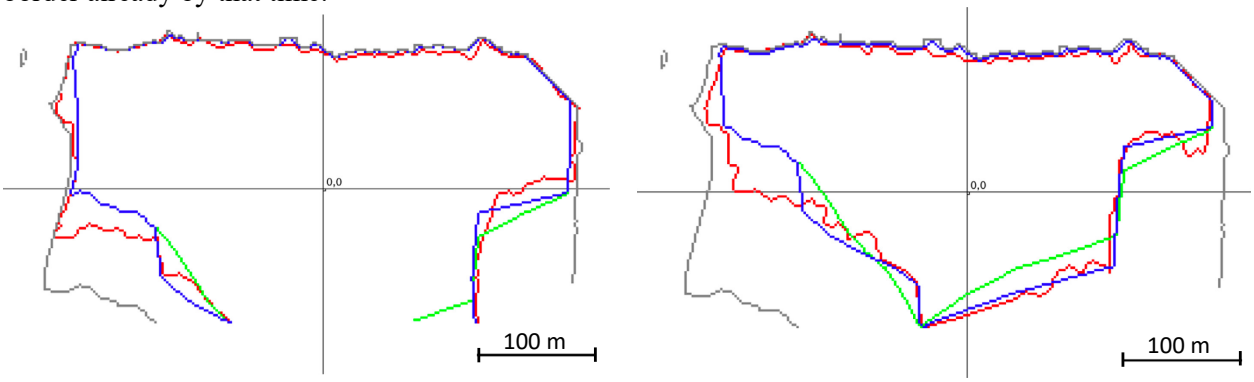

(a) (b)

Figure 5. Prescribed Fire Simulation for the Flight2 Time Period: (a) Simulated fires at Loop 3 ending time; (b) Simulated fires at Loop 4 ending time. In the figures, the gray fire front is the Loop2 fire front (initial condition); the red fire front is the real fire front; the blue fire front is the simulated fire front using the estimated ignition procedure; the green fire front is the simulated fire front using the "non-stopping average speed" ignition procedure.

Figure 6 shows the burned areas of the two simulated fires over time. The burned area is calculated as the areas burned from the beginning of the simulation starting from the Loop2 fire shape. We record the

accumulated burned areas every 30 seconds, as well as at the Loop3 ending time and Loop4 ending time. The figure also shows the burned areas of the real fire at the Loop3 ending time and Loop4 ending time, which are calculated as the areas that the real fire spreads from the Loop 2 fire shape to the Loop 3 and Loop 4 fire shapes shown in Figure 4, respectively. Since the fire maps at the Loop 3 ending time and Loop 4 ending time are the only data we have for the real fire, we do not have burned area data for other time instances for the real fire. The figure shows that the burned areas using the estimated ignition procedure are closer to those of the real fire compared to the "non-stopping average speed" ignition procedure. This is consistent with what is observed from Figure 5. We note that more advanced measurement metrics, such as arrival time agreement and shape agreement (Filippi et al. 2014, Salis et al. 2016), may be used to provide more detailed quantification for the differences between the simulated and real fires. We will consider these metrics in future work.

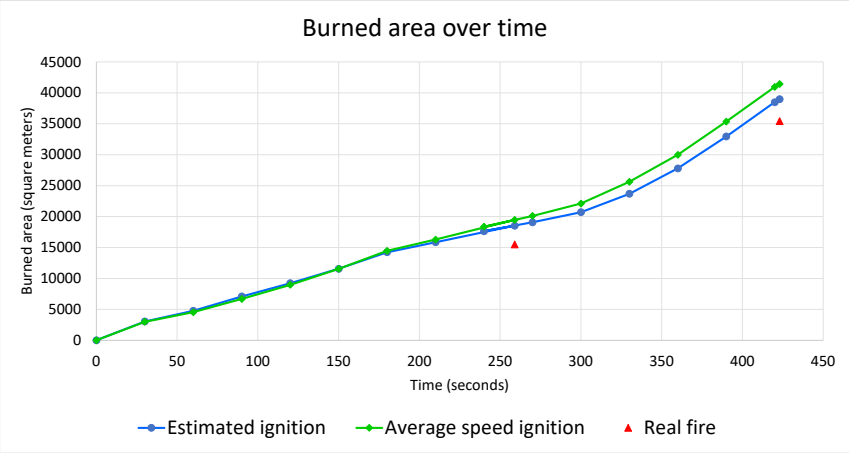

Figure 6: Burned area over time starting from Flight 2's Loop2 ending time

3.2 Prescribed Fire Simulation from the Very Beginning

This experiment simulates the prescribed fire from the very beginning when the fire was first ignited to Flight2's Loop 4 ending time (total 2617 seconds). Similarly, we estimate the major ignition activities of the fire setting teams and specify them using the ignition plan specification. For the time period between Flight2's Loop 2 ending time and Loop 4 ending time, we reuse the same estimated ignition procedure from Section 3.1. Table 2 shows the ignition plan specification.

Table 2: Ignition Plan Specification from the Very Beginning

The estimated ignition procedure		
<Team> *0 // west team* *O; W; 0.4; continuous* *W; P; 0.3; continuous* <Wait> 140 *Q; Q; 0.3; continuous* <Wait> *280* *R; S; 0.3; continuous* <Wait> *255* *S; A; 1.5; continuous* <Wait> *120* *A; M; 0.45; continuous* </Team>	<Team> 1 // east team O*; E; 0.4; continuous* <Wait> *180* E*; F; 0.2; continuous* <Wait> *345* F*; C; 1.3; continuous* C*; D; 1.3; continuous* <Wait> *200* D*; M; 1.3; continuous* </Team>	<Team> 2 // northeast corner team <Wait> *1340* H*; K; 0.7; continuous* </Team>

Figure 7 illustrates the ignition procedure of the three teams specified by the ignition plan specification. The coordinates of the specific locations are: O=(150, 139); W=(0, 139); P=(0, 100); Q=(22, 100); R=(22,

80); S=(22, 14); E=(264,139); F=(264, 30); H=(260, 80); K=(220, 130). The locations A, C, D, M are the same as being described in Section 2.3 (location B is on the segment F-C and is not shown in Figure 7). Note that the west team skipped two segments at the west borders of the fire area. This is shown by the missed lines between P-Q and Q-R in Figure 7. For the east team, one of the crew members ignited fires cutting across the northeast corner while the rest of the team ignited the east border. Since this is a parallel ignition activity to the east team ignition, we use a separate team (Team 2 in the specification) to specify this part of the ignition, which is indicated by the orange line on the northeast corner of the field.

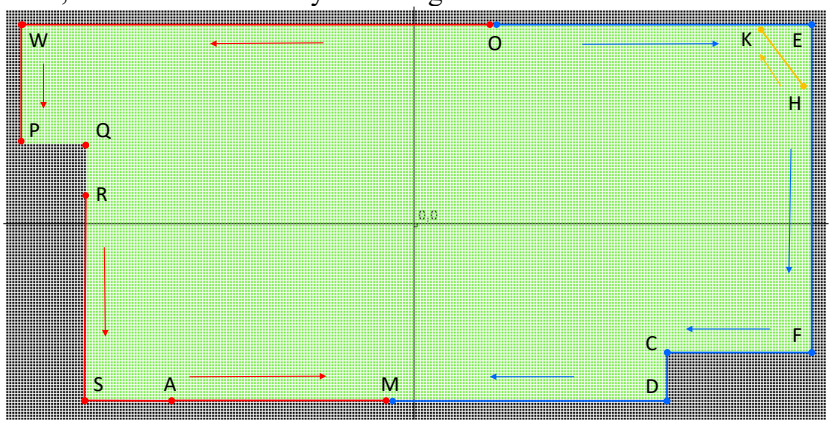

Figure 7. Illustration of the Ignition Procedure. Team 0's ignition route is shown in red; Team 1's ignition route is shown in blue; Team 2's ignition route is shown in orange. Ignition segments are displayed as solid lines; directions of movement are indicated by the arrows.

For comparison purpose, we also consider a "non-stopping average speed" ignition scenario, where the two teams ignite all the segments along the fire setting routes using the average speeds, and the two teams arrive at the merging point at the same time (Flight2's Loop 4 ending time). No stopping and no skipping are involved. The average speeds are calculated by dividing the overall route distances by the time (2617 seconds). The west team's average speed is 0.31 m/s, and the east team's average speed is 0.285 m/s. The northeast corner team is the same as being specified in Table 2. To save space we omit the detailed specification of this "non-stopping average speed" ignition scenario.

Figure 8 shows the simulated fire fronts at Flight2's Loop 2 ending time, Loop 3 ending time, and Loop 4 ending time. It can be seen that the two ignition procedures result in different fire front shapes. The fire front from the estimated ignition procedure (blue) matches the main features of the real fire front very well. There are large differences between the fire front from the "non-stopping average speed" ignition procedure and the real fire front. For example, its fire front on the east and southeast sides spread much faster than the real fire did because the team keeps igniting the fire without stopping.

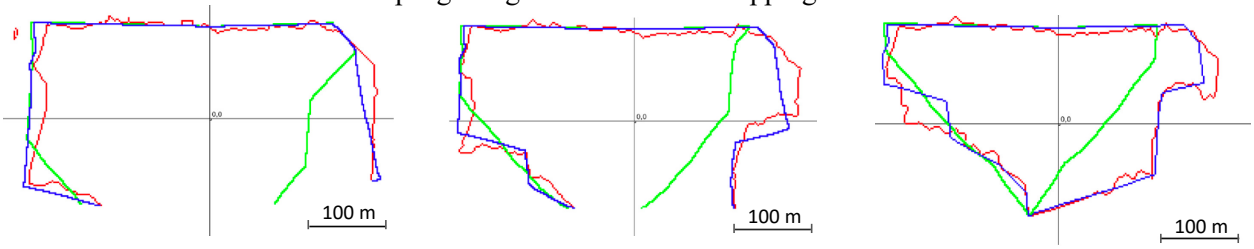

(a) Loop 2 ending time (b) Loop 3 ending time (c) Loop 4 ending time

Figure 8: Prescribed Fire Simulation from the Very Beginning. In the figures, the red fire front is the real fire front; the blue fire front is the simulated fire front using the estimated ignition procedure; the green fire front is the simulated fire front using the "non-stopping average speed" ignition procedure.

Figure 9 shows the burned areas of the two simulated fires in every 120 seconds, as well as at Flight1's Loop 1, Loop 3, Loop 4 ending time, and Flight2's Loop 2, Loop 3, and Loop 4 time. The real fire's burned areas at those times are displayed too. The burned areas are calculated in a similar way as described in Section 3.1, starting from the very beginning when the fire was first ignited. The figure shows that the burned areas from the estimated ignition procedure match closely to those from the real fire. The burned areas from the "non-stopping average speed" ignition procedure have large differences during the latter part of the event. The difference reaches 18,664 square meters at Flight2's Loop 4 ending time. The different results from the two ignition procedures show that prescribed fire ignition has a large impact on a prescribed fire's fire growth behavior. Different ignition procedures can result in significantly different fire fronts. This shows the importance of having the right ignition plans for specific prescribed burn events.

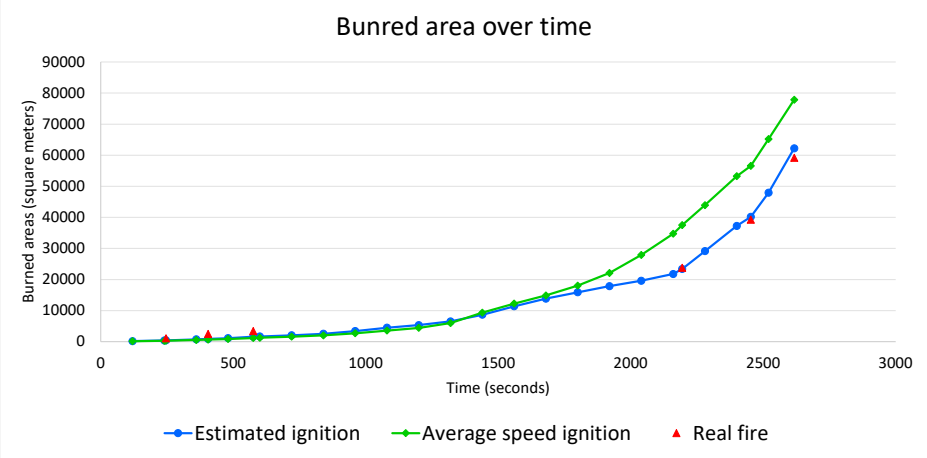

Figure 9: Burned area over time starting from the very beginning

4. Discussion

The experiments presented in Section 3.1 and 3.2 show that the fire setting procedure has a significant impact on the fire growth behavior of a prescribed fire. Each experiment considers the estimated ignition plan and a baseline "non-stopping average speed" ignition plan. The two ignition plans start and end at the same time and follow exactly the same routes; the only difference is the timing and ignition speed for the different segments. In both experiments, the two ignition plans lead to significantly different spatial-temporal fire growth behaviors. Furthermore, there are major differences between the observed fire shape and the simulated fire shape using the baseline "non-stopping average speed" ignition plan. An in-depth analysis of the sensitivity of the simulation result to the different parameters of the ignition plans is beyond the scope of this paper. Nevertheless, we can expect that changing other parameters of the ignition plan, such as the number of teams, ignition routes, and granularity of ignition segments, will have similar or even larger impacts on the fire growth behavior.

These results have implications for both prescribed burn operations and simulation of prescribed fires. On the one hand, they show that a well-developed fire setting plan is important for carrying out a prescribed burn event. Simulation would be a useful tool to support such planning. On the other hand, when simulating the spatial-temporal behavior of a prescribed fire it is necessary to have adequate information about the fire setting procedure. Technologies such as GPS sensors or body cameras may be used to record the locations and actions of fire setting teams. Such data would be useful to re-construct the fire setting procedures to help post-event simulation and analysis.

While the simulations using the estimated ignition plans match the real fire well, differences between the two still exist. This is likely due to the following reasons. First, the ignition procedures used in the simulations are estimated based on the UAS data. They may differ from the actual ignition procedure. This can lead to differences between the simulated fires and the real fire. Second, this work assumes homogenous

fuel conditions across the whole area and estimates the fuel characteristics (e.g., fuel moisture content) based on an average FROS (see Section 2.4). The estimated fuel characteristics may not accurately reflect the actual fuels in the field. Furthermore, the spatial heterogeneity of the fuel that exists in the real field is not considered in this work, which can lead to simulation results that are different from the real fire spread. Third, the wind data used by the simulations were measured by a 3D sonic anemometer near the burning field. These data did not capture the atmospheric dynamics inside the fire area. This aspect of fire-atmospheric interaction is not modeled by the DEVS-FIRE model, which can also contribute to the differences between the simulated fires and the real fire.

Fire front location is one of the most important data for prescribed fires. UAS makes it possible to collect real-time and high-resolution fire front data in a safe and low-cost manner. In this paper, the fire front maps are stitched from individual thermal images collected by UAS. This approach brings an error in representing the fire front because the individual images were taken at different times while the fire was spreading. The parts of the fire map stitched from earlier images are likely to have more errors because more time have elapsed from when the images were taken. A future research task is to apply advanced data assimilation techniques (see e.g., Xue et al. (2012)) that take into consideration the different observation times of the thermal images to construct the fire maps.

While UAS is a valuable tool for prescribed fire data collection, adequate planning of UAS' flights is essential in order to collect the most useful data. One aspect of the planning is related to the UAS flight time, i.e., when to fly and land the UAS. This planning is important because most small UAS have limited flight time (mainly due to the battery constraint), while a prescribed fire may last for hours. For the prescribed fire considered in this paper, the UAS had two flights that cover the early part of the fire event. However, due to battery depletion it was not able to fly and cover the last part of the event when the fire spread the fastest. Another aspect of the planning is related to the path planning of the UAS. This is important because the UAS could monitor only a portion of the fire area. Thus, what path the UAS flies is directly related to which part of the fire area is monitored. From a data collection point of view, it is more important to pay more attention to the areas that have the most active fire spread (e.g., the head of the fire as opposed to the tail of the fire). A future research task is to use prescribed fire simulations to help the planning of UAS' flying path for collecting the most useful data.

To conclude, this paper presents a case study of prescribed fire simulation using data from UAS-based sensing. A systematic approach for modeling and simulating prescribed fires with dynamic ignitions is developed. The developed approach is applied to a real prescribed fire using data from UAS-based sensing. Real-time fire data acquired by UAS fill a critical gap of data collection for prescribed fires. The high spatiotemporal resolution of UAS data makes it possible to align simulations with real prescribed fires, and thus greatly enhance the capabilities of simulation. While this study is based on a grassland fire, the principles of the developed approach are applicable to other types of prescribed fires, such as shrubland fires. We note that collecting UAS data in other landscapes, such as in a mountain environment, could be more challenging due to the complex terrain and canopy that may exist. Future work includes applying the UAS-based sensing to prescribed fires in various environments and carry out simulations to study more prescribed fires.

Acknowledgements

The authors would like to thank Sheena Parsons, Dr. Dean Kettle, Bruce Johanning and Vaughn Salisbury from Kansas Biological Survey for their help with fire experiments and UAS data collection. This work was supported by the US Department of Agriculture (USDA) National Institute of Food and Agriculture (NIFA) under grant number 2019-67021-29011, 2019-67021-28992, and 2019-67021-28993.

References

Andrews, P. L. (2012). Modeling wind adjustment factor and midflame wind speed for Rothermel's surface fire spread model. Gen. Tech. Rep. RMRS-GTR-266. Fort Collins, CO: US Department of Agriculture, Forest Service, Rocky Mountain Research Station. 39 p.. 2012;266

Beachly, E. M. (2017). An Unmanned Aerial System for Prescribed Fires, MS Thesis, University of Nebraska – Lincoln, 2017

Bugwood Center (1989). Firing Techniques - A Guide for Prescribed Fire in Southern Forests. United States Department of Agriculture, Forest Service Southern Region, Technical Publication R8-TP 11. Available from: https://www.bugwood.org/pfire/techniques.cfm.

Clements, C. B., S. Zhong, S. Goodrick, J. Li, B. E. Potter, X. Bian, W. E. Heilman, J. J. Charney, R. Perna, M. Jang, D. Lee, M. Patel, S. Street, and G. Aumann, (2007). Observing the dynamics of wildland grass fires – FireFlux – a field validation experiment. Bull. Amer. Meteorol. Soc., 88, 1369–1382, doi:10.1175/BAMS-88-9-1369.

Clements, C. B., A. K. Kochanski, D. Seto, B. Davis, C. Camacho, N. P. Lareau, J. Contezac, J. Restaino, W. E. Heilman, S. K. Krueger, B. Butler, R. D. Ottmar, R. Vihnanek, J. Flynn, J.-B. Filippi, T. Barboni, D. E. Hall, J. Man- del, M. A. Jenkins, J. O'Brien, B. Hornsby, and C. Teske, (2019). The FireFlux II experiment: a model-guided field experiment to improve understanding of fire-atmosphere interactions and fire spread. International Journal of Wildland Fire, 28, 308–326, doi:10.1071/WF18089.

Dahl, N., Xue, H., Hu, X., & Xue, M. (2015). Coupled fire–atmosphere modeling of wildland fire spread using DEVS-FIRE and ARPS. Natural Hazards. 2015 Jun 1;77(2):1013-35.

Fayad, J., Morandini, F., Accary, G., Chatelon, F., Wandon, C., Burglin, A., Rossi, L., Marcelli, T., Cancellieri, D., Cancellieri, V., Morvan, D., Meradji, S., Pieri, A., Planelles, G., Costantini, R., Briot, P., & Rossi, J. (2023). A Study of Two High Intensity Fires across Corsican Shrubland. Atmosphere 2023, 14, 473. https://doi.org/10.3390/atmos14030473

Fernandes, P. M., & Botelho, H. S. (2003). A review of prescribed burning effectiveness in fire hazard reduction. International Journal of wildland fire. 12(2):117-28.

Filippi, J.-B., Mallet, V., & Nader, B. (2014). Representation and evaluation of wildfire propagation simulations. Int J Wildland Fire, 23 (2014), pp. 46-57

Filippi, J.-B., Pialat, X., & Clements, C. B. (2013). Assessment of ForeFire/Meso-NH for wildland fire/atmosphere coupled simulation of the FireFlux experiment. Proceedings of the Combustion Institute, 34, 6233–2640, doi:10.1016/j.proci.2012.07.022.

Finney, M. A., & McAllister, S. S. (2011). A review of fire interactions and mass fires. Journal of Combustion. 2011 Apr; 2011.

Gowravaram, S., Chao, H., Zhao, T., Parsons, S., Hu, X., Xin, M., Flanagan, H., & Tian, P. (2022). Prescribed Grass Fire Evolution Mapping and Rate of Spread Measurement Using Orthorectified Thermal Imagery from a Fixed-Wing UAS, International Journal of Remote Sensing, 43:7, pp. 2357-2376

Hiers, J.K., O'Brien, J.J., Varner, J.M., Butler, B.W., Dickinson, M., Furman, J., Gallagher, M., Godwin, D., Goodrick, S.L., Hood, S.M., Hudak, A., Kobziar, L.N., Linn, R., Loudermilk, E.L., McCaffrey, S., Robertson, K., Rowell, E.M., Skowronski, N., Watts, A.C., & Yedinak, K.M. (2020). Prescribed fire science: the case for a refined research agenda, Fire Ecology, volume 16, Article number: 11

Hu, X., Sun, Y., & Ntaimo, L. (2012). DEVS-FIRE: design and application of formal discrete event wildfire spread and suppression models. Simulation. 88(3):259-79.

Hu, X., Ge, M. (2021). Modeling and Simulating Prescribed Fire Ignition Techniques. In 2021 Annual Modeling and Simulation Conference (ANNSIM'21); 2021

Johansen, R. W. (1987). Ignition patterns & prescribed fire behavior in southern pine stands. Georgia Forestry Commission-Georgia Forest Research Paper 72: 1-8.

Kelso, J. K., Mellor, D., Murphy, M. E., & Milne, G. J. (2015). Techniques for evaluating wildfire simulators via the simulation of historical fires using the Australis simulator. International Journal of Wildland Fire. 2015 Jun 11;24(6):784-97.

Kim, E.H., Yang, K., & Tran, M.N. (2012). Thermal-image-based wildfire spread simulation using a linearized model of an advection-diffusion-reaction equation. Simulation, 88 (9), pp. 1093-1115

Kochanski, A. K., M. A. Jenkins, J. Mandel, J. D. Beezley, C. B. Clements, and S. Krueger, (2013). Evaluation of WRF- SFIRE performance with field observations from the FireFlux experiment. Geoscientific Model Development, 6, 1109–1126, doi:10.5194/gmd-6-1109-2013.

Linn, R.R., Goodrick, S.L., Brambilla, S., Brown, M.J., Middleton, R.S., O'Brien, J.J., & Hiers, J.K. (2020) QUIC-fire: A fast-running simulation tool for prescribed fire planning, Environmental Modelling & Software, 125: 104616-. https://doi.org/10.1016/j.envsoft.2019.104616

Martin, R. E., & Dell, J. D. (1978). Planning for prescribed burning in the inland northwest. Department of Agriculture, Forest Service, Pacific Northwest Forest and Range Experiment Station.

Matthias, B., Sadler, R., Wittkuhn, R.S., Mccaw, L., & Grierson, P. (2009). "Long-term impacts of prescribed burning on regional extent and incidence of wildfires - Evidence from 50 years of active fire management in SW Australian forests", Forest Ecology and Management, Volume 259, Issue 1, 5 December 2009, Pages 132-142

Morandini, F., Silvani, X., Rossi, L., Santoni, P.A., Simeoni, A., Balbi, J.H., Rossi, J.L., & Marcelli, T. (2006). Fire spread experiment across Mediterranean shrub: influence of wind on flame front properties. Fire Safety Journal 41(3), 229–235. doi:10.1016/J.FIRESAF.2006.01.006

Ntaimo, L., Hu, X., & Sun, Y. (2008). DEVS-FIRE: Towards an integrated simulation environment for surface wildfire spread and containment. Simulation. 84(4):137-55.

Rothermel, R. C. (1972). A mathematical model for predicting fire spread in wildland fuels. Intermountain Forest & Range Experiment Station, Forest Service, US Department of Agriculture; 1972

Salis, M., Arca, B., Alcasena, F., Arianoutsou, M., Bacciu, V., Duce, P., Duguy, B., Koutsias, N., Mallinis, G., Mitsopoulos, I., Moreno,J.M., Perez, J.R., Rodriguez, I., Xystrakis, F., Zavala, G., & Spano, D. (2016). Predicting wildfire spread and behavior in Mediterranean landscapes, Int. J. Wildland Fire, 25 (2016), pp. 1015-1032

Santoni, P.A., Simeoni, A., Rossi, J.L., Bosseur, F., Morandini, F., Silvani, X., Balbi, J.H., Cancellieri, D., & Rossi, L. (2006). Instrumentation of wildland fire: characterisation of a fire spreading through a Mediterranean shrub. Fire Safety Journal 41(3), 171–184. doi:10.1016/J.FIRESAF.2005.11.010

Sargent, R. G. (2013). Verification and validation of simulation models. Journal of Simulation, 2013. 7(1): 12-24

Scott, J. H., & Burgan, R. E. (2005). Standard fire behavior fuel models: a comprehensive set for use with Rothermel's surface fire spread model. Gen. Tech. Rep. RMRS-GTR-153. Fort Collins, CO: U.S. Department of Agriculture, Forest Service, Rocky Mountain Research Station; 2005.

Sullivan, A. L. (2009a). Wildland surface fire spread modelling, 1990–2007. 1: Physical and quasi-physical models. International Journal of Wildland Fire. 2009 Jun 29;18(4):349-68.

Sullivan, A. L. (2009b). Wildland surface fire spread modelling, 1990–2007. 2: Empirical and quasi-empirical models. International Journal of Wildland Fire. 2009 Jun 29;18(4):369-86.

Toivanen, J., Engel, C. B., Reeder, M. J., Lane, T. P., Davies, L., Webster, S., & Wales, S. (2019). Coupled Atmosphere-Fire Simulations of the Black Saturday Kilmore East Wildfires With the Unified Model. Journal of Advances in Modeling Earth Systems. 2019 Jan;11(1):210-30.

Trunfio, G. A., Ambrosio, D., Rongo, R., Spataro, W., & Di Gregorio, S. (2011). A New Algorithm for Simulating Wildfire Spread through Cellular Automata. ACM Trans. Modeling and Computer. Simulation. 2011, 22, 1–26

Twidwell, D., Allen, C. R., Detweiler, C., Higgins, J., Laney, C., & Elbaum, S. (2016). Smokey comes of age: unmanned aerial systems for fire management. Frontiers in Ecology and the Environment. 14(6):333-9.

USDA (n.d.). Prescribed Fire. https://www.fs.usda.gov/managing-land/prescribed-fire.

USGS. (n.d.). Science Data Catalog (SDC). https://data.usgs.gov/datacatalog/data/USGS:b7e353d2-325f-4fc6-8d95-01254705638a

Waldrop, T. A., & Goodrick, S. L. (2012). Introduction to prescribed fires in Southern ecosystems. Science Update SRS-054. Asheville, NC: US Department of Agriculture Forest Service, Southern Research Station.

Xue, H., Gu, F., Hu, X. (2012). Data Assimilation Using Sequential Monte Carlo Methods in Wildfire Spread Simulation, The ACM Transactions on Modeling and Computer Simulation (TOMACS), Vol. 22, No. 4, Article No. 23

Zeigler, B. P., Praehofer, H., Kim, T. G. (2000). Theory of modeling and simulation, 2nd ed. NewYork: Academic Press; 2000